Automatic Detection of Comets from Multi-Spectral Infrared Images

Anonymous WACV submission

Paper ID ****

Abstract

This paper addresses the challenge of detecting comets of various shapes and sizes in large-scale multispectral astronomical surveys. We propose a deep learning-based framework, based on Faster-RCNN, that is designed to handle images of multiple and arbitrary wavelenghts. Such a framework may seamlessly adapt to current and future observation missions. We also release the first annotated image dataset for benchmarking and comparison of comet detection algorithms. The proposed pipeline is tested on the 4-band images of the large-scale astronomical survey NEOWISE. We report greater than 80% average precision across a 16-fold cross-validation. Furthermore, we show that utilizing information from multiple infrared wavelengths provides an 170% increase in precision when compared to the same network trained on single-wavelength images.

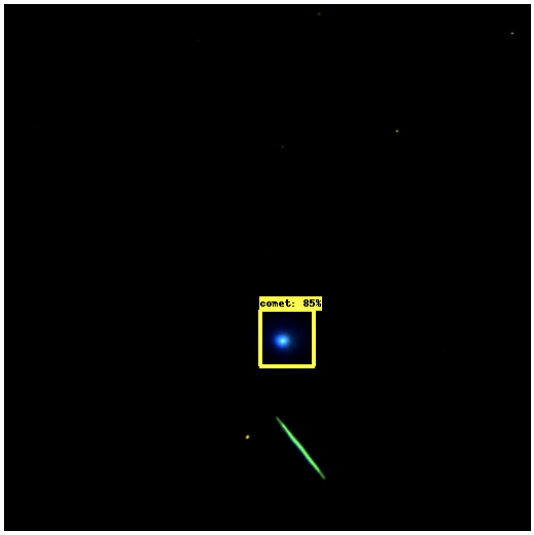

Figure 1: Succesful Detection of Comet 29P

1. Introduction

Object detection is a key problem in astronomy. It is made more challenging by multispectral image data, where objects have distinct appearances in different wavelengths. As astronomical surveys increase in data volume, human eye-search no longer becomes possible; object detection must be automated. Deep Neural Networks (DNNs) provide a promising alternative to eye-search. In the setting of natural images, DNN architectures such as Faster-RCNN [15] and YOLO [14] have become popular for achieving high accuracy on detection tasks such as facial recognition [17] and pedestrian detection for self-driving cars [1]. In this pilot study, we aim to adapt this technology to detect bright comets in NEOWISE infrared images.

NEOWISE's current detection architecture combines an automatic pipeline with human eye-search [6]. In general, near earth objects (NEOs) such as asteroids and comets appear in these images as point sources, as they are small compared to the telescope field of view. Point sources are easy to detect using statistical models such as the MDET detection algorithm used by NEOWISE [6] because they are structurally simple. Occasionally, however, bright comets pass through WISE's field of view in varied shapes and sizes, often taking up much of the image. These comets are currently found by eye-search, as their complicated structure prevents them from being detected by algorithms such as MDET [6]. We propose a Faster-RCNN [15] DNN as an alternative method to detect bright and complicated comets.

Images from infrared astronomical surveys such as NEOWISE differ significantly in properties to the natural images that DNNs such as Faster-RCNN were designed and trained for. We investigate the ability of Faster-RCNN to handle multi-modal infrared astronomical images, and the necessary adaptations for the images themselves.

The contributions of our work are:

- A proof of concept for the use of DNN in astronomical detection pipelines for comets.

- An open-source codebase [1] that extends Tensorflow's object detection library [9] to be used in an astronomical setting.
- The first data set of annotated multispectral images of comets.

2. Previous works

Some automated methods for comet detection have been proposed, e.g. in [6, 21]. The work in [6] has a very similar setting to ours, as Cutri et al. aimed at detecting asteroids and comets from a combination of all bands of WISE images. In a Bayesian framework, they used a maximum likelihood profile fitting procedure [6, 5]. This allowed looking for point sources that have a high enough signal-to-noise ratio and the expected point-like structure. A limitation of this method is that it cannot recognize larger comets where the tail, coma, and nucleus structures are visible and create a more complex appearance.

Zoghbi et al. in [21] proposed to use deep learning, namely a CNN and LSTM neural network, to detect meteor showers from low light ground-based video observations. Although the setting and data are quite different from ours, this is the only other work we know of that uses deep learning methods to detect comets.

2.1. Object Detection in Astronomical Surveys

In other domains of astronomy, computer vision is used quite routinely to detect and classify objects, and deep learning methods are quickly becoming increasingly common. The reference tool with the astronomical community for detection and classification of a large variety of objects is SExtractor [5]. This tool detects sources in astronomical images by convolving a preprocessed image with a template frame and then thresholding to determine high activation image regions. Neural networks are used in SExtractor for star/galaxy separation, but these networks are small and not suitable for more complicated detection tasks. Other works, e.g. [4, 7, 3] also focused on stars/galaxy separation with small neural networks. Most methods, such as [7], use model fitting for multispectral image data. More recently, authors used deep neural networks to detect objects that are difficult to identify with eye-search in very large observation surveys, such as far and young galaxies [10] or exoplanets [16, 13].

2.2. Deep Learning Based Detection in Multispectral Images

Deep learning has become a standard framework for object detection and classification, with methods such as Faster-RCNN [15] or YOLOv3 [14], achieving near-human performance in all but real time. In this work, we build on the Faster-RCNN framework, due to its popularity, ease of use, and high performance.

Although deep learning was initially designed to work with natural images, it has since then be extended to other image domains, such as depth images [20] and medical imaging modalities [19]. Some works investigated using multiple bands as input to deep neural networks. Zhou et al. [20] investigated the image preprocessing and multiple bands' encoding that best allow CNNs to exploit a combination of RGB and depth images, in a pedestrian detection application. They train a DNN comprised of two networks, one taking RGB data as input and the other depth data. The final prediction is based off of a combination of the predictions of each network. Vakalopoulou et al. [18] and Hamida et al. [8] join multispectral images into a combined feature vector before training in the context of mapping land and buildings from satellite images. We follow their recommendation to merge multispectral data before training.

3. Methodology

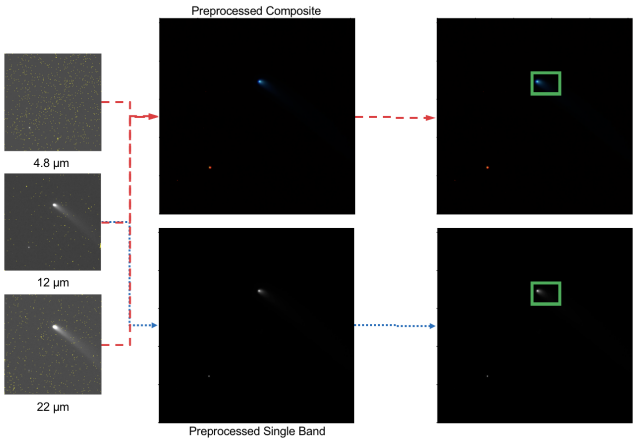

Figure 2: Overview of our proposed comet detection pipeline

3.1. Data

To the best of our knowledge, there is no publicly available dataset for training and benchmarking comet detection methods. We introduce here a new annotated dataset that will be released at the end of the project.

Our dataset is made up of images of 11 comets (Figure 3) and 5 large non-comet objects (Figure 4) which could be easily confused for comets, such as bright stars, planets, and large asteroids. The cometary images also contain stars, satellites, and other potential sources of false detection. Each image is available in 4 infrared bands. Example

[1] https://github.com/nasa/BrightComets

of images of our dataset are presented in Figs. 3, 4. These images are brightened so the comets are more visible.

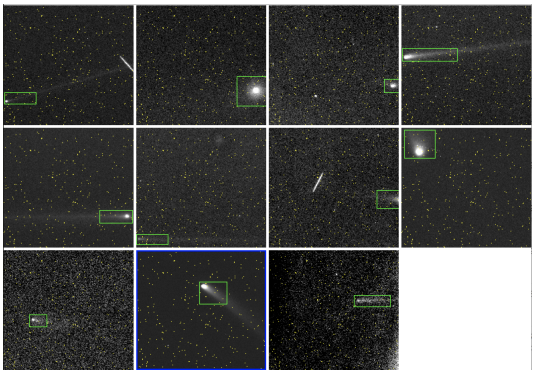

Figure 3: Our Comet Images with Annotation, Left to Right, Top to Bottom: 10P, 29P, 30P, 65P, 81P, 116P, 118P, 2006 W3, 2010 H2, 2007 Q3, 2007 N3

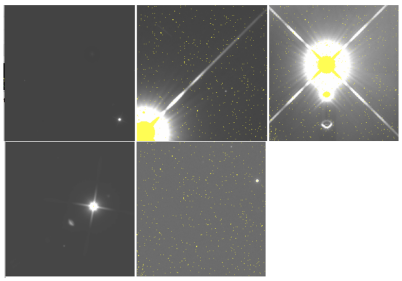

Figure 4: Our Non-Comet Images, Left to Right, Top to Bottom: Alpha Boo, Jupiter, Mars, R Dor, 81 Terpischore

The images were collected from the IRSA catalog of WISE images [6]. They were taken by the WISE satellite every six seconds in four wavelengths of infrared, 3.4, 4.6, 12 and 22 μm [6]. In this study, we compare band three, the 12 μm band, to a combination of bands two through four, stacked as an RGB as explained in Section 3.2.

In data from the WISE All-Sky data release, the NEOWISE mission has detected 164 comets during the WISE All-Sky data release, 11 of which we deemed visible enough for this study [2, 6]. These 11 comets provide 319 sets of images that were selected for the dataset. Each set of images contains four images of the same location of the sky, each taken in a different infrared wavelength. This makes for a total of 1276 annotated images before data augmentation. To artificially increase the size of the dataset, all combinations of horizontal flips, vertical flips and 90 degree rotations are applied to the images.

Annotations were created manually by a comet expert astronomer. Each comet was annotated with a bounding box surrounding the nucleus, coma, and the visible tail of the comet, as shown in Fig. 3. Because comets are varied in shape and size, and also don't have clearly defined edges, we had to make a decision about how to bound the comets. We aimed at bounding the maximal visible area of the comet while minimizing the amount of extraneous information in the box. We always included the comet's nucleus and coma. As for the comet's tail, it was included when bright, but left out when it too drastically increased the size of the bounding box. This naturally leads to some ambiguity in the annotations that may have an adversarial effect when training DNNs. This effect will need to be assessed in future works.

Our dataset also includes annotations for bright non-comet objects including stars and planets. These annotations were not used in this study, as we focused on comet only detection. Nevertheless, these extra annotations will be released with the dataset, to allow further studies on multi-object detection and classification.

3.2. Preprocessing

The images taken by WISE often have corrupted pixels and artifacts, as can be see in Fig. 3 for example. They also often suffer from low contrasts combined with high dynamic ranges on the order of 10^4. Therefore, the first image preparation steps of our framework aim at correcting these defects to obtain an image quality that is comparable to that of natural images. This strategy was demonstrated in [12] to improve the domain transfer ability of DNNs.

Corrupted pixels are given in the original images with a NaN designation. We remove these pixels by replacing them with the median neighboring pixel. Then, the dynamic range is normalized to the range [0-255] to maintain consistency with images that the DNN was pre-trained on. To remove remaining artifacts such as salt and pepper background noise, tiny stars, and faint satellite trails, we send the entire image through a median filter.

Since comets are always bright objects in a dark field in these infrared images, we truncate the dim pixels of the image and set them to 0. Specifically we fit a Gaussian to the image's histogram and truncated pixels below two standard deviations of the gaussian's mean. We visually verified that this entirely affected background pixels, while it didn't alter the appearance of comets, stars, or other bright objects. Finally, we center the pixel values around 0 to match the pre-training conditions of our neural network.

As previously mentioned, we train our neural network on both $12\mu m$ data as well as composite images of multispectral data. To create composite images of the $4.8, 12, and 22\mu m$ infrared bands, the images are stacked into a single RGB image. Specifically, in the new image, the $4.8\mu m$ band is stored in the red channel, the $12\mu m$ band in the green channel, and the $22\mu m$ band in the blue channel. The result of this transformation can be seen in Fig. 6.

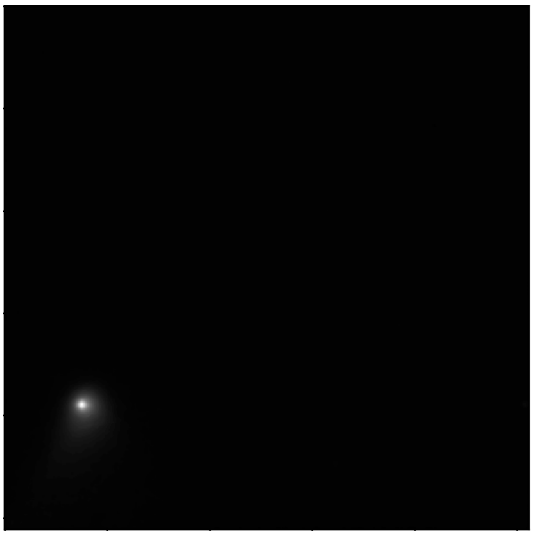

Figure 5: Preprocessed $22\mu m$ Image of Comet C/2006 W3

Figure 6: Preprocessed Composite Image of Comet C/2006 W3

3.3. Deep neural network

We used a TensorFlow implementation of the Faster-RCNN with Inception Resnet [9, 15] pre-trained on the COCO dataset[2]. We chose this network because of its relatively high accuracy for near real-time results, making it a convenient architecture for use in this pilot study, where our main goal is to prove the potential of using deep neural networks for this type of data.

The COCO dataset contains over 300K images of dogs, planes, traffic lights, people, and over 80 other categories of commonly seen objects [11]. While these images are in an entirely different domain from the astronomical images we studied, we investigate the ability of the DNN to these image and problem domains.

We fine-tune our neural network with a constant learning rate of $3 * 10^{-4}$ for 2000 iterations using the built in retraining functionality of the Tensorflow object detection library [9]. All model parameters of this Faster-RCNN implementation were kept unchanged. In future studies, it will be important to experiment with different network architectures and more training iterations.

4. Evaluation/Experiments

We evaluate the performance of our framework for comets detection on our annotated dataset of real images. We experiment with both a network trained on only the 12 μm band as well as a network trained on a composite image of 4.6, 12, and 22 μm bands.

All our evaluations use a 16-fold cross validation strategy, with each fold being the entire set of images of one object. This allows assessing the networks' ability to detect individual objects it has never seen before.

Detection quality is evaluated by the precision (P) and recall (R) measures. R is the percentage of comets that were positively detected, and P is calculated as

$$P = \frac{1}{num\_images} \sum_{i=1}^{num\_images} P_i \qquad (1)$$

where for every image i,

$$P_i = \frac{true\_positives}{true\_positives + false\_positives} \qquad (2)$$

We count predictions as proposals returned by the DNN with attached score greater than a threshold which we will refer to as the score threshold

We count a prediction as a positive detection when its intersection over union (IoU) with regards to ground truth is greater than a threshold which we will refer to as the IoU threshold.

We present precision and recall results at all IoU and score thresholds for both multispectral and single wavelength images in Figures 7a, 8a, 7b, and 8b. In each of these images, pixel intensity represents mean AP or mean AR over all 16 folds of cross validation.

Decreasing IoU threshold increases recall and precision dramatically on both multispectral and single band images. This is expected, as decreasing the IoU threshold is relaxing the constraints of our detection problem. Thus, more predictions are accepted as true positives. It is to be noted that the confidence threshold does not vary, hence the constraint on correctness of predictions remains the same. This

[2] https://github.com/tensorflow/models/blob/master/research/object_detection/g3doc/detection_model_zoo.md

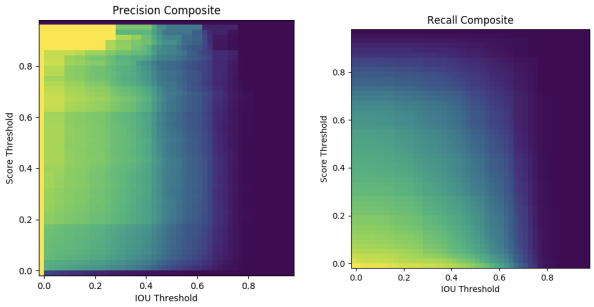

(a) (b)

Figure 7: P (a) and R (b) on Multispectral composite Images at Various IoU and Score Thresholds

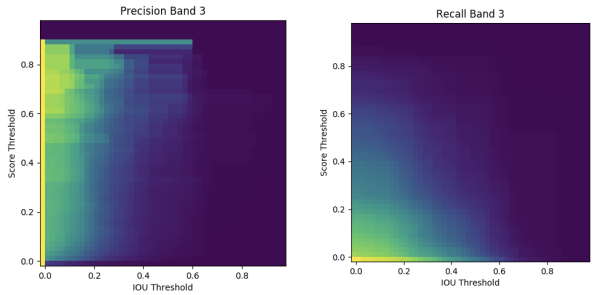

(a) (b)

Figure 8: P (a) and R (b) on $22\mu m$ Images at Various IoU and Score Thresholds

explains that precision keeps increasing at the same time as recall.

Increasing the confidence score at which we accept proposals generally increases precision and decreases recall by putting a stronger constraint on correctness of predictions. We plot this trend at fixed IoU thresholds of 0.1 and 0.5 in in Figs. 9 and 10. We also display the confidence threshold for peak points along the P vs. R curves which are the optimal trade-off between precision and recall which we defined as

$$\max P + R \tag{3}$$

subject to the constraint that P and R are both greater than 0.1.

The 0.5 IoU threshold is commonly used for computing AP in detection problems. However, given the difficulty in defining the boundaries of the comets (see discussion in Section 3.1), this threshold may be too strict in our case.

The 0.1 threshold puts much milder constraints on the exact localization of the comet, thus making the problem of the exact definition of its boundaries less dominant. While a low localization score may be concerning in the setting of natural image detection, we are focusing more on the network's ability to correctly classify comets than on its ability

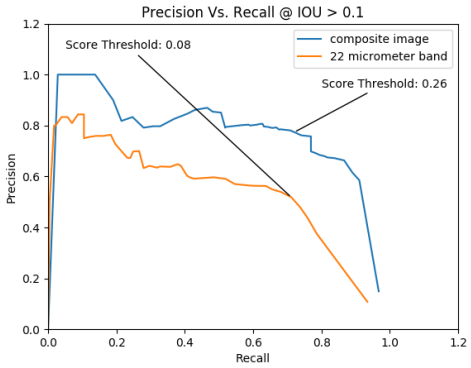

Figure 9: P vs. R at Various Score Thresholds, IoU > 0.1

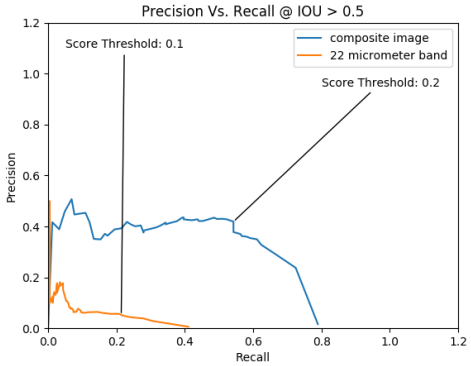

Figure 10: P vs. R at Various Score Thresholds, IoU > 0.5

to bound them. This is in great part due to the fact that the exact definition of the comet's boundaries is an ill-posed problem due to the fuzziness of its coma and especially tail.

Between IoU thresholds of 0.1 and 0.5, there is a smooth decrease in both AP and AR metrics, which can be seen in the heat maps, Figs. 7 and 8. This is certainly due to the aforementioned differences in the strength on constraints for accurate localization.

At IoU threshold of 0.5, multispectral images perform ~~on~~ 3.89 and 3.99 times better than single band images in AR and AP, respectively. This shows that the network has a drastically easier time localizing when multispectral data is provided. In the IoU > 0.1 setting, multispectral images still performed 1.72 and 1.29 times better in AR and AP, respectively.

Multispectral images performed far better at all thresholds, especially for higher IoU thresholds. This is most probably due to the method being able the exploit more information from the multiple bands of the data.

5. Conclusion and future work

We demonstrate that deep learning is a simple and effective strategy for tackling comet detection in multispectral and astronomical images. Furthermore, we show in an astronomical setting that providing multispectral image data can provide drastic performance improvements when compared to single channel detection. We also introduce a new dataset to be used for the training and benchmarking of detection systems on bright cometary bodies. Finally, we include a codebase that extends Tensorflow's object detection library [9] to be used for the processing of astronomical data and training DNNs on such data.

Future work for classifying bright comets includes improvements of the training procedure (e.g. more data), and experimenting with different DNN architecture and composition strategies for multispectral images, to find a more optimal setting than used in this proof-of-concept study

References

[1] Deep learning strong parts for pedestrian detection. In ICCV, 2015.

[2] J. M. Bauer, T. Grav, Y. R. Fernández, A. K. Mainzer, E. A. Kramer, J. R. Masiero, T. Spahr, C. R. Nugent, R. A. Stevenson, K. J. Meech, R. M. Cutri, C. M. Lisse, R. Walker, J. W. Dailey, J. Rosser, P. Krings, K. Ruecker, E. L. Wright, and the NEOWISE Team. Debiasing the NEOWISE Cryogenic Mission Comet Populations. , 154:53, Aug. 2017.

[3] E. Bertin. Classification of astronomical images with a neural network. Science with Astronomical Near-Infrared Sky Surveys, page 4951, 1994.

[4] E. Bertin. Mining pixels: The extraction and classification of astronomical sources. ESO ASTROPHYSICS SYMPOSIA Mining the Sky, page 353371, 2001.

[5] E. Bertin and S. Arnouts. SExtractor: Software for source extraction. , 117:393–404, June 1996.

[6] R. M. Cutri, E. L. Wright, T. Conrow, J. Bauer, D. Benford, H. Brandenburg, J. Dailey, P. R. M. Eisenhardt, T. Evans, S. Fajardo-Acosta, J. Fowler, C. Gelino, C. Grillmair, M. Harbut, D. Hoffman, T. Jarrett, J. D. Kirkpatrick, D. Leisawitz, W. Liu, A. Mainzer, K. Marsh, F. Masci, H. McCallon, D. Padgett, M. E. Ressler, D. Royer, M. F. Skrutskie, S. A. Stanford, P. L. Wyatt, D. Tholen, C. W. Tsai, S. Wachter, S. L. Wheelock, L. Yan, R. Alles, R. Beck, T. Grav, J. Masiero, B. McCollum, P. McGehee, M. Papin, and M. Wittman. Explanatory Supplement to the WISE All-Sky Data Release Products. Technical report, Mar. 2012.

[7] N. Drory. Yet another object detection application (yoda). Astronomy Astrophysics, 397(1):371379, Nov 2002.

[8] A. B. Hamida, A. Benoit, P. Lambert, L. Klein, C. B. Amar, N. Audebert, and S. Lefvre. Deep learning for semantic segmentation of remote sensing images with rich spectral content. In 2017 IEEE International Geoscience and Remote Sensing Symposium (IGARSS), pages 2569–2572, July 2017.

[9] J. Huang, V. Rathod, C. Sun, M. Zhu, A. Korattikara, A. Fathi, I. Fischer, Z. Wojna, Y. Song, S. Guadarrama, and K. Murphy. Speed/accuracy trade-offs for modern convolutional object detectors. CoRR, abs/1611.10012, 2016.

[10] M. Huertas-Company, J. R. Primack, A. Dekel, D. C. Koo, S. Lapiner, D. Ceverino, R. C. Simons, G. F. Snyder, M. Bernardi, Z. Chen, and et al. Deep learning identifies high-z galaxies in a central blue nugget phase in a characteristic mass range. The Astrophysical Journal, 858(2):114, 2018.

[11] T. Lin, M. Maire, S. J. Belongie, L. D. Bourdev, R. B. Girshick, J. Hays, P. Perona, D. Ramanan, P. Dollár, and C. L. Zitnick. Microsoft COCO: common objects in context. CoRR, abs/1405.0312, 2014.

[12] A. Paiement. Integrated registration, segmentation, and interpolation for 3d/4d sparse data. 14:6–8, 01 2015.

[13] K. A. Pearson, L. Palafox, and C. A. Griffith. Searching for exoplanets using artificial intelligence. Monthly Notices of the Royal Astronomical Society, 474(1):478491, 2017.

[14] J. Redmon, S. Divvala, R. Girshick, and A. Farhadi. You only look once: Unified, real-time object detection. arXiv, 2015.

[15] S. Ren, K. He, R. Girshick, and J. Sun. Faster r-cnn: Towards real-time object detection with region proposal networks. IEEE Transactions on Pattern Analysis & Machine Intelligence, 39:1137–1149, 2017.

[16] C. J. Shallue and A. Vanderburg. Identifying exoplanets with deep learning: A five-planet resonant chain around kepler-80 and an eighth planet around kepler-90. The Astronomical Journal, 155(2):94, 2018.

[17] X. Sun, P. Wu, and S. Hoi. Face detection using deep learning: An improved faster rcnn approach. Neurocomputing, 299:42–50, 2018.

[18] M. Vakalopoulou, K. Karantzalos, N. Komodakis, and N. Paragios. Building detection in very high resolution multispectral data with deep learning features. In 2015 IEEE International Geoscience and Remote Sensing Symposium (IGARSS), pages 1873–1876, July 2015.

[19] Y. Yu, H. Lin, J. Meng, X. Wei, H. Guo, and Z. Zhao. Deep transfer learning for modality classification of medical images. Information, 8(3), 2017.

[20] K. Zhou, A. Paiement, and M. Mirmehdi. Detecting humans in rgb-d data with cnns. 2017 Fifteenth IAPR International Conference on Machine Vision Applications (MVA), 2017.

[21] S. Zoghbi, M. D. Cicco, A. Ordonez, and A. Stapper.